On the Magnetic and Mössbauer Spectroscopic Characterization of $EuPd_2Sb_2$

Inga Schellenberg, Matthias Eul, and Rainer Pöttgen

Institut für Anorganische und Analytische Chemie, Westfälische Wilhelms-Universität Münster, Corrensstraße 30, 48149 Münster, Germany

Reprint requests to R. Pöttgen. E-mail: pottgen@uni-muenster.de

Z. Naturforsch. **2010**, *65b,* 18 – 22; received October 2, 2009

The $CaBe_2Ge_2$-type antimonide $EuPd_2Sb_2$ (*P*4/*nmm*, a = 462.43(7), c = 1056.1(2) pm) was synthesized by induction melting of the elements in a sealed tantalum tube. Temperature-dependent magnetic susceptibility measurements have revealed Curie-Weiss behavior with an experimental magnetic moment of 7.93(1) μ_B/Eu atom, indicating stable divalent europium. $EuPd_2Sb_2$ orders antiferromagnetically at T_N = 4.5(2) K as is also evident from almost full hyperfine field splitting (B_h = 19.5 T) in the ^{151}Eu Mössbauer spectrum at 4.2 K.

Key words: Europium, Antimonides, Mössbauer Spectroscopy

Introduction

The EuM_2Sb_2 antimonides have been reported for M = Mg, Mn, Ni, Cu, Zn, Pd, Cd, and Pt [1 – 14]. Depending on the transition metal component they crystallize with five different structure types. With M = Mg [8], Mn [2, 14], Zn [3], and Cd [7] the EuM_2Sb_2 antimonides adopt the trigonal $CaAl_2Si_2$ type structure, space group $P\bar{3}m1$, with a slightly distorted tetrahedral coordination for the M and Sb atoms. Similar transition metal coordination occurs in the $ThCr_2Si_2$-type structure of $EuNi_2Sb_2$ [1]. $EuPd_2Sb_2$ [5] and $EuCu_2Sb_2$ [6] crystallize with a superstructure of the $ThCr_2Si_2$ type due to a different ordering of the transition metal and antimony atoms in the $[M_2Sb_2]$ networks. A more complicated situation occurs for $EuPt_2Sb_2$ [11]. Splitting of some reflections in the Guinier powder patterns indicates a deviation from tetragonal symmetry, and the $EuPt_2Sb_2$ structure is most likely similar to that of $SrPt_2As_2$ and $EuPt_2As_2$ [11].

Magnetic susceptibility measurements of the EuM_2Sb_2 antimonides with M = Mg, Cd, Zn, Cu, and Mn show stable divalent europium. $EuCd_2Sb_2$ [7] orders ferromagnetically at T_C = 12 K with a spin reorientation at T_N = 7.8 K. Thermoelectric measurements [13] indicate that $EuCd_2Sb_2$ is a *p*-type conductive material. This is similar for $EuZn_2Sb_2$ [4, 9, 10] (T_N = 13.3 K) which shows a high *p*-type Seebeck coefficient and good thermoelectric properties. Simple antiferromagnetic ordering has been observed for $EuMg_2Sb_2$ [8] (T_N = 8.2 K) and $EuCu_2Sb_2$ [6] (T_N = 6 K).

A very interesting example is $EuMn_2Sb_2$ [14] which shows two independent magnetic substructures. The manganese magnetic moments order magnetically at around 600 K, while the europium atoms order antiferromagnetically at the much lower Néel temperature of 9 K. In continuation of our systematic investigations of $ThCr_2Si_2$- and $CaBe_2Ge_2$-related intermetallics with magnetic cations [15 – 18] we were interested in the behavior of $EuPd_2Sb_2$. The magnetic properties and a Mössbauer spectroscopic characterization of this antimonide are reported herein.

Experimental Section

Synthesis

Starting materials for the preparation of $EuPd_2Sb_2$ were sublimed ingots of europium (Johnson Matthey), palladium powder (Heraeus) and antimony shots (ABCR), all with stated purities better than 99.9 %. The air- and moisture-sensitive europium ingots were kept under argon prior to the reaction. The argon was purified before with titanium sponge (870 K), silica gel and molecular sieves. The elements were weighed in the ideal 1:2:2 atomic ratio and sealed in a tantalum tube under an argon pressure of 800 mbar in an arc melting apparatus [19]. The tantalum tube was subsequently placed in the water-cooled sample chamber of an induction

Table 1. Fitting parameters of ^{121}Sb and ^{151}Eu Mössbauer spectroscopic measurements of $EuPd_2Sb_2$. Numbers in parentheses represent the statistical errors in the last digit. (δ) isomer shift; (Γ) experimental line width; (ΔE_Q) electric quadrupole splitting; (B_h) magnetic hyperfine field. Numbers marked with an asterisk were fixed during the fitting procedure.

Source	T (K)	δ (mm s^{-1})	Γ (mm s^{-1})	ΔE_Q (mm s^{-1})	B_h (T)
^{121}Sb	77	−8.74(2)	3.07(8)	−0.28(1)	
	4.2	−8.67(3)	3.25(1)	−0.28(1)	
^{151}Eu	298	−11.67(1)	2.70(4)	0.0*	
	77	−11.77(1)	2.96(2)	0.0*	
	4.2	−11.75(4)	3.70(7)	0.0*	19.5(1)

furnace [20] (Hüttinger Elektronik, Freiburg, Germany, Typ TIG 2.5/300), heated to 1680 K, and kept at that temperature for 10 min. Finally, the temperature was lowered to 1180 K, and the sample was annealed at that temperature for another 3 h and then allowed to cool within the furnace after the power was switched off. The temperature was controlled by a Sensor Therm Methis MS09 pyrometer with an accuracy of ±30 K. No reaction with the container material was observed. The polycrystalline sample has a golden color and is stable in air for weeks. Small single crystals exhibit metallic lustre.

X-Ray powder diffraction

The polycrystalline sample was characterized through a Guinier powder pattern (Cu$K_{\alpha 1}$ radiation, α-quartz: a = 491.30, c = 540.46 pm as internal standard). The Guinier camera was equipped with an imaging plate technique (Fujifilm, BAS-READER 1800). The lattice parameters (Table 1) were obtained through a least-squares routine. The correct indexing was ensured through comparison of the experimental pattern with a calculated one [21]. The refined data compare well with the ones reported by Hofmann and Jeitschko (a = 462.9(1), c = 1056.8(2) pm) [5].

Susceptibility measurements

The magnetic measurements were carried out on a Quantum Design Physical Property Measurement System (PPMS) using the VSM option. For the measurements, 16.950 mg of the $EuPd_2Sb_2$ sample was packed in kapton foil and attached to the sample holder rod for measuring the magnetic properties in the temperature range 2.2 – 300 K with magnetic flux densities up to 80 kOe.

Mössbauer spectroscopy

The 21.53 keV transition of ^{151}Eu with an activity of 130 MBq (2 % of the total activity of a ^{151}Sm:EuF_3 source) and a $Ba^{121m}SnO_3$ source were used for the Mössbauer spectroscopic experiments, which were conducted in the usual transmission geometry. The measurements were performed with a commercial helium bath cryostat. The temperature of the absorber was varied between 4.2 K and r. t., while the source was kept at room temperature. The temperature was controlled by a resistance thermometer (±0.5 K accuracy). The sample was enclosed in a small PVC container at a thickness corresponding to about 10 mg of the Mössbauer-active element/cm^2.

Results and Discussion

Crystal chemistry

$EuPd_2Sb_2$ crystallizes with the tetragonal $CaBe_2Ge_2$-type structure, space group *P*4/*nmm*. A view on the crystal structure approximately along the y axis is presented in Fig. 1. The palladium and antimony atoms build up a three-dimensional [Pd_2Sb_2] network with tetrahedral $Pd1Sb_4$ and square-pyramidal $Pd2Sb_5$ coordination. The Pd–Sb distances within the network range from 260 to 268 pm. For single-crystal data and a detailed crystal chemical discussion of $EuPd_2Sb_2$ we refer to [5]. Details of the many $BaAl_4$ / $ThCr_2Si_2$-related structures, and considerations of chemical bonding in this family of compounds, are given in [15, 22 – 24, and references cited therein].

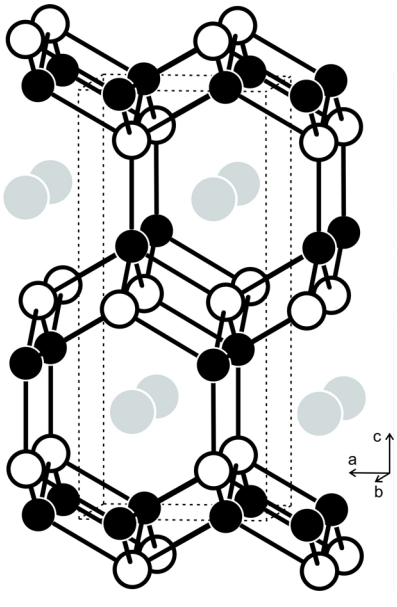

Fig. 1. View of the $EuPd_2Sb_2$ structure approximately along the crystallographic y axis. Europium, palladium, and antimony atoms are drawn as medium grey, black filled, and open circles, respectively. The three-dimensional [Pd_2Sb_2] network is emphasized.

^{121}Sb and ^{151}Eu Mössbauer spectroscopic characterization

The ^{121}Sb and ^{151}Eu Mössbauer spectra of the antimonide $EuPd_2Sb_2$ taken at r. t., 77 and 4.2 K are presented in Figs. 2 and 3 together with transmission integral fits. The corresponding fitting parameters are listed in Table 1. For the ^{121}Sb measurements the spectra could be well reproduced with single antimony sites, although the structure contains two crystallographically independent antimony atoms. In the fits a quadrupole splitting of around -0.28 mm s^{-1} has been used. Most likely the two antimony subspectra are similar and the broad natural line width of antimony hampers higher resolution.

The ^{121}Sb isomer shift compares very well with the ones determined for other RET_2Sb_2 (*RE* = Eu, Yb; *T* = Zn, Mn) compounds [14]. According to the ionic formula splittings, *e. g.* $Eu^{2+}(2Mn^{2+})(2Sb^{3-})$, these compounds contain Sb^{3-} pnictide anions. These Zintl anions also occur in antimonide oxides *RE*MnSbO [25] and in the series Yb*T*Sb [26], and the experimental isomer shifts are comparable to those given in an overview of different antimony compounds by Lippens [27].

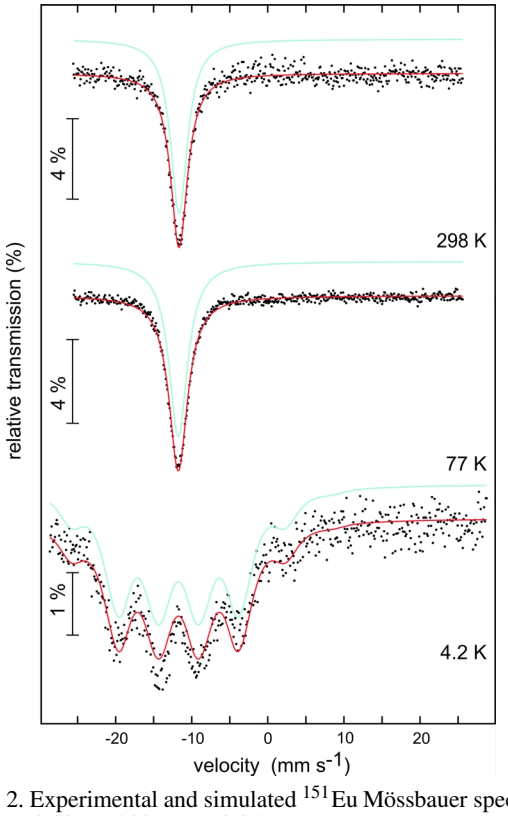

Fig. 2. Experimental and simulated ^{151}Eu Mössbauer spectra of $EuPd_2Sb_2$ at 298, 77 and 4.2 K.

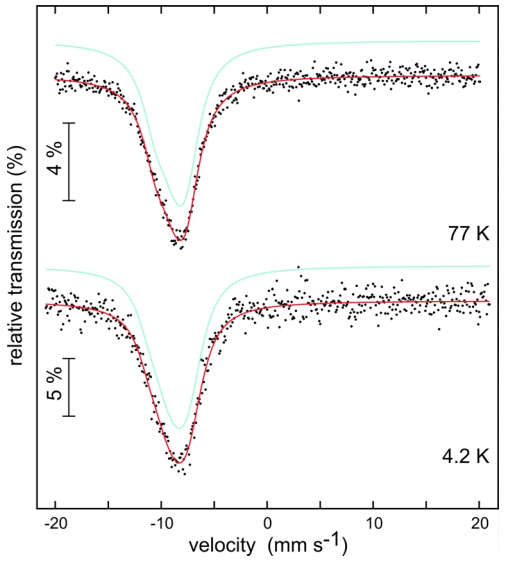

Fig. 3. Experimental and simulated ^{121}Sb Mössbauer spectra of $EuPd_2Sb_2$ at 77 and 4.2 K.

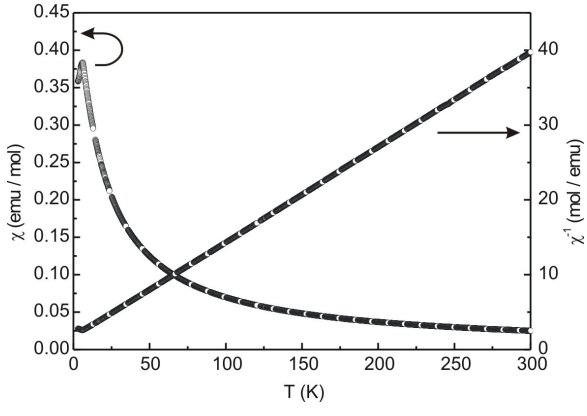

Fig. 4. Temperature dependence of the magnetic susceptibility (χ and χ^{-1} data) of $EuPd_2Sb_2$ measured at 10 kOe.

At 4.2 K we observe no transferred hyperfine field for $EuPd_2Sb_2$ which could have been expected to result from the antiferromagnetic ordering of this compound (*vide infra*). This behavior was observed for $EuMn_2Sb_2$ and $EuZn_2Sb_2$ which crystallize in the $CaAl_2Si_2$ structure type, where transferred hyperfine fields of around 9 T could be detected at the antimony nuclei [14].

The europium spectra are composed of one major resonance at isomer shift values corresponding to

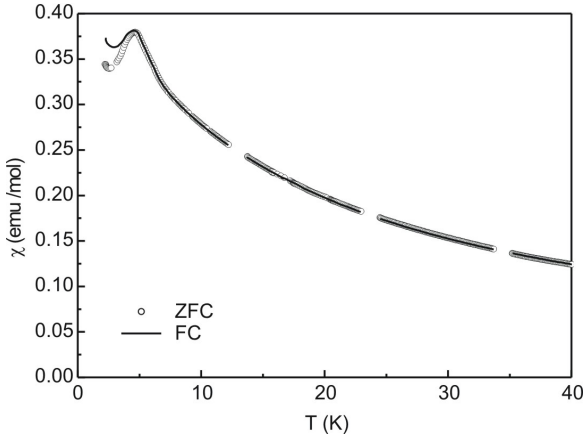

Fig. 5. Susceptibility measurements at 100 Oe of $EuPd_2Sb_2$ in the zero-field-cooled (ZFC) and field-cooled (FC) mode.

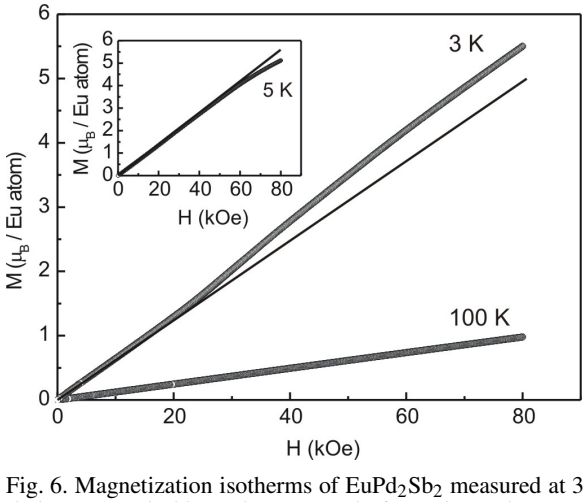

Fig. 6. Magnetization isotherms of $EuPd_2Sb_2$ measured at 3 (below T_N) and 100 K (above T_N). The inset shows the magnetization isotherm at 5 K (just above T_N). The straight black lines are inserted as a visual help to accentuate the metamagnetic step below T_N and the curvature just above T_N.

divalent europium atoms. No quadrupole interaction could be determined in the fitting procedure. At 4.2 K the europium magnetic moments are in an ordered state leading to a magnetic hyperfine field of 19.5 T acting on the nuclear spin levels resulting in clearly visible Zeeman splittings. The observed hyperfine field is smaller than the ones determined for other RET_2Sb_2 compounds (B_h = 26 – 29 T) [14] as the ordering temperature (4.5 K) is just slightly higher than the lowest available temperature (4.2 K) of our experimenal setup. Thus, no full splitting is observed.

Magnetic properties

The $\chi(T)$ and $\chi^{-1}(T)$ data of $EuPd_2Sb_2$ measured at 10 kOe are shown in Fig. 4. In the temperature range of 25–300 K the data could be fitted with the Curie-Weiss law, revealing an effective magnetic moment of μ_{eff} = 7.93(1) μ_B / Eu atom and a Weiss constant of $\theta_P = -12.7(2)$ K. The effective magnetic moment almost perfectally coincides with the theoretical free ion value for Eu^{2+} of 7.94 μ_B, thus indicating purely divalent europium in the compound. The negative θ_P is indicative of antiferromagnetic interactions. In the low-temperature region antiferromagnetic ordering is evident from the $\chi(T)$ data. To determine the exact Néel-temperature (T_N) low-field susceptibility measurements were performed.

The susceptibility in an external field of 100 Oe was first measured in a zero-field-cooled and additionally in a field-cooled state in the temperature range of 2.2 – 40 K (Fig. 5). By these means the ordering temperature was determined at T_N = 4.5(2) K.

Fig. 6 displays the magnetization isotherms taken at different temperatures. The magnetization isotherms above the ordering temperature, *viz.* at 55 and 100 K, show a linear increase of magnetization with the application of an external field, as is expected for a paramagnetic material. Close to the ordering temperature, the isotherm at 5 K reveals a slight curvature at high fields. Below the ordering temperature, *viz.* at 3 K, the magnetization isotherm displays a weak metamagnetic step starting at around 25 kOe. The magnetization isotherm at 3 K shows a saturation magnetization of approximately 5.5 μ_B / Eu atom at 80 kOe, about 1.5 μ_B lower than the maximum theoretical value of $g_J \times S$ = 7 μ_B / Eu atom. The M(H) behavior below the ordering temperature is non-hysteretic, and together with the observed metamagnetic behavior manifests the antiferromagnetic ground state.

Acknowledgement

This work was financially supported by the Deutsche Forschungsgemeinschaft.

[1] R. Marchand, W. Jeitschko, *J. Solid State Chem.* **1978**, *24*, 351.

[2] R. Rühl, W. Jeitschko, *Mater. Res. Bull.* **1979**, *14*, 513.

[3] P. Klüfers, H. Neumann, A. Mewis, H.-U. Schuster, *Z. Naturforsch.* **1980**, *35b*, 1317.

[4] G. Zwiener, H. Neumann, H.-U. Schuster, *Z. Naturforsch*. **1981**, *36b*, 1195.
[5] W. K. Hofmann, W. Jeitschko, *Monatsh. Chem*. **1985**, *116*, 569.
[6] J. Dünner, A. Mewis, M. Roepke, G. Michels, *Z. Anorg. Allg. Chem*. **1995**, *621*, 1523.
[7] A. Artmann, A. Mewis, M. Roepke, G. Michels, *Z. Anorg. Allg. Chem*. **1996**, *622*, 679.
[8] F. Wartenberg, Chr. Kranenberg, R. Pocha, D. Johrendt, A. Mewis, R.-D. Hoffmann, B. D. Mosel, R. Pöttgen, *Z. Naturforsch*. **2002**, *57b*, 1270.
[9] F. Weber, A. Cosceev, A. Nateprov, C. Pfleiderer, A. Faißt, M. Uhlarz, H. von Löhneysen, *Physica B* **2005**, *359 – 361*, 226.
[10] F. Weber, A. Cosceev, S. Drobnik, A. Faißt, K. Grube, A. Nateprov, C. Pfleiderer, M. Uhlarz, H. von Löhneysen, *Phys. Rev. B* **2006**, *73*, 014427.
[11] A. Imre, A. Hellmann, G. Wenski, J. Graf, D. Johrendt, A. Mewis, *Z. Anorg. Allg. Chem*. **2007**, *633*, 2037.
[12] H. Zhang, J.-T. Zhao, Y. Grin, X.-J. Wang, M.-B. Tang, Z.-Y. Man, H.-H. Chen, X.-X. Yang, *J. Chem. Phys*. **2008**, *129*, 164713.
[13] H. Zhang, L. Fang, M.-B. Tang, H.-H. Chen, X.-X. Yang, X. Guo, J.-T. Zhao, Y. Grin, *Intermetallics* **2010**, *18*, 193.
[14] I. Schellenberg, M. Eul, W. Hermes, R. Pöttgen, *Z. Anorg. Allg. Chem*. **2010**, *636*, 85.
[15] D. Kußmann, R. Pöttgen, U. Ch. Rodewald, C. Rosenhahn, B. D. Mosel, G. Kotzyba, B. Künnen, *Z. Naturforsch*. **1999**, *54b*, 1155.
[16] D. Niepmann, R. Pöttgen, *Intermetallics* **2001**, *9*, 313.
[17] M. Rotter, M. Tegel, D. Johrendt, I. Schellenberg, W. Hermes, R. Pöttgen, *Phys. Rev. B* **2008**, *78*, 020503.
[18] M. Tegel, M. Rotter, V. Weiss, F. M. Schappacher, R. Pöttgen, D. Johrendt, *J. Phys.: Condens. Matter* **2008**, *20*, 452201.
[19] R. Pöttgen, Th. Gulden, A. Simon, *GIT Labor-Fachzeitschrift* **1999**, *43*, 133.
[20] D. Kußmann, R.-D. Hoffmann, R. Pöttgen, *Z. Anorg. Allg. Chem.* **1998**, *624*, 1727.
[21] K. Yvon, W. Jeitschko, E. Parthé, *J. Appl. Crystallogr*. **1977**, *10*, 73.
[22] C. Zheng, R. Hoffmann, *J. Solid State Chem*. **1988**, *72*, 58.
[23] D. Johrendt, C. Felser, O. Jepsen, O. K. Andersen, A. Mewis, J. Rouxel, *J. Solid State Chem*. **1997**, *130*, 254.
[24] E. Parthé, L. Gelato, B. Chabot, M. Penzo, K. Cenzual, R. Gladyshevskii, *TYPIX-Standardized Data and Crystal Chemical Characterization of Inorganic Structure Types*, Gmelin Handbook of Inorganic and Organometallic Chemistry, 8th edition, Springer, Berlin, **1993**.
[25] I. Schellenberg, T. Nilges, R. Pöttgen, *Z. Naturforsch*. **2008**, *63b*, 834.
[26] R. Mishra, R. Pöttgen, R.-D. Hoffmann, Th. Fickenscher, M. Eschen, H. Trill, B. D. Mosel, *Z. Naturforsch*. **2002**, *57b*, 1215.
[27] P. E. Lippens, *Solid State Commun*. **2000**, *113*, 399.